Supporting Information

Hydroxylamine Intermediate Governs Selectivity in Nitrite Hydrogenation on Pd-based Catalysts for Sustainable Water Treatment

Janek Betting,[a] Yardthip Preedawichitkun,[b] Tawan Sooknoi, [b] Leon Lefferts,, [a] Jimmy A. Faria Albanese*, [a]*

[a]Catalytic Processes and Materials Group, Department for Chemical Engineering, Faculty of Science and Technology, MESA+ Institute for Nanotechnology, University of Twente, Enschede 7500 AE, The Netherlands.

[b]Department of Chemisty, Faculty of Science, King Mongkut's Institute of Technology Ladkrabang, Chalongkrung Road, Ladkrabang, Bangkok 10520, Thailand

Table of Content

1. Internal mass transport limitations

To exclude possible internal mass transport limitations, the catalytic NO_2^- conversion experiment was conducted with catalyst with different support particle size. Therefore, the catalyst was pelletized, crushed, and sieved in different fractions. The results indicate the absence of internal mass transport limitations when using particles below 38 µm.

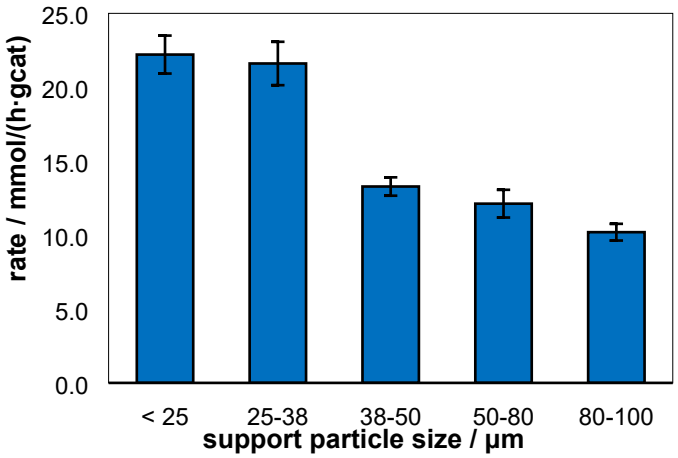

Figure 1: NO_2^- hydrogenation rate of Pd/Al_2O_3 of different support particle sizes showing no significant activity difference between < 25 and 25-38 µm. For catalytic testing presented in this manuscript catalyst particles < 38 µm were used. Reaction conditions: 0.8 mmol/L KNO_2, 10 mg Pd/Al_2O_3, 300 mL H_2O, 80:10:10 mL/min H_2:CO_2:He, RT, 600 rpm.

2. Concentration Profiles over time:

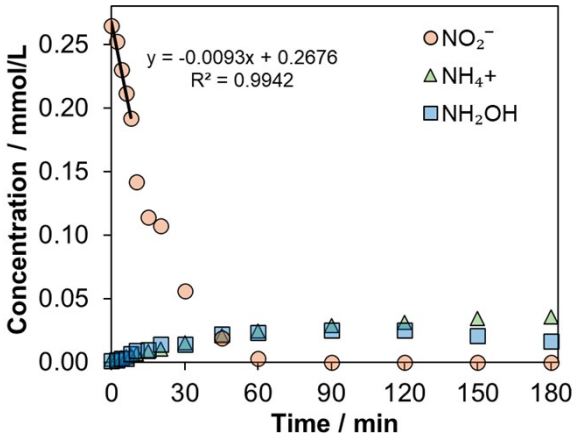

Figure 2: Typical concentration profile of NO2- hydrogenation reaction. Reaction conditions: 10 mg Pd/Al_2O_3, 300 mL H_2O, 80:10:10 mL/min H_2:CO_2:He, RT, 600 rpm.

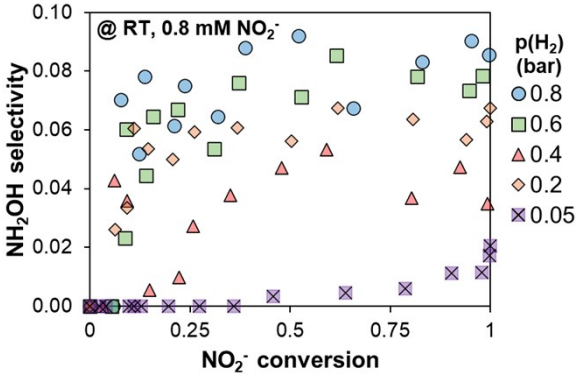

Figure 3: NH_2OH selectivity as function of NO_2^- conversion. Reaction conditions: 300 mL H_2O, 10 mg Pd/Al_2O_3, 10 mL/min CO_2, 5-80 mL/min H_2 and He to balance to 100 mL/min total flow, RT, 600 rpm.

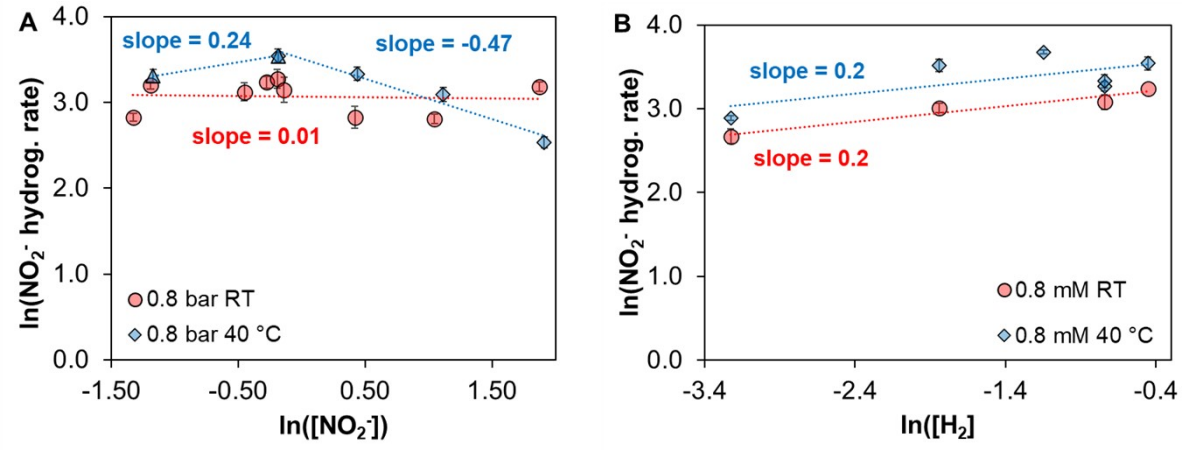

Figure 4: Effect of NO_2^- (**A**) and H_2 concentration (**B**) on the NO_2^- hydrogenation rate on Pd/Al_2O_3 at RT and 40 °C. Reaction conditions: 300 mL H_2O, 10 mg Pd/Al_2O_3, 10 mL/min CO_2, 5-80 mL/min H_2 and He to balance to 100 mL/min total flow, RT (red circle) or 40 °C (blue diamond), 600 rpm.

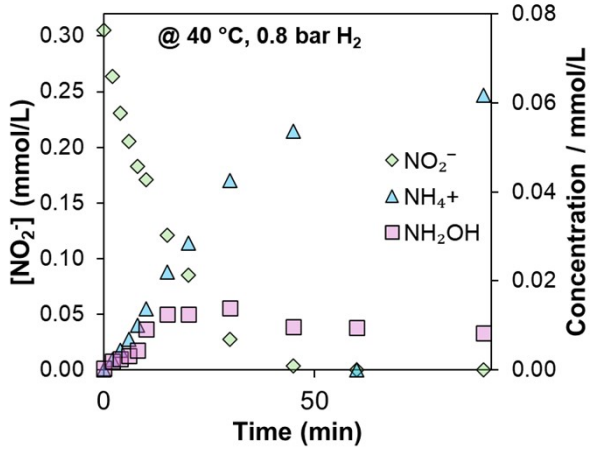

Figure 5: Typical concentration profile of NO_2^- hydrogenation at 40 °C. Reaction conditions: 300 mL H_2O, 10 mg Pd/Al_2O_3, 0.8 mmol/L KNO_2, 10 mL/min CO_2, 5-80 mL/min H_2 and He to balance to 100 mL/min total flow, RT, 600 rpm.

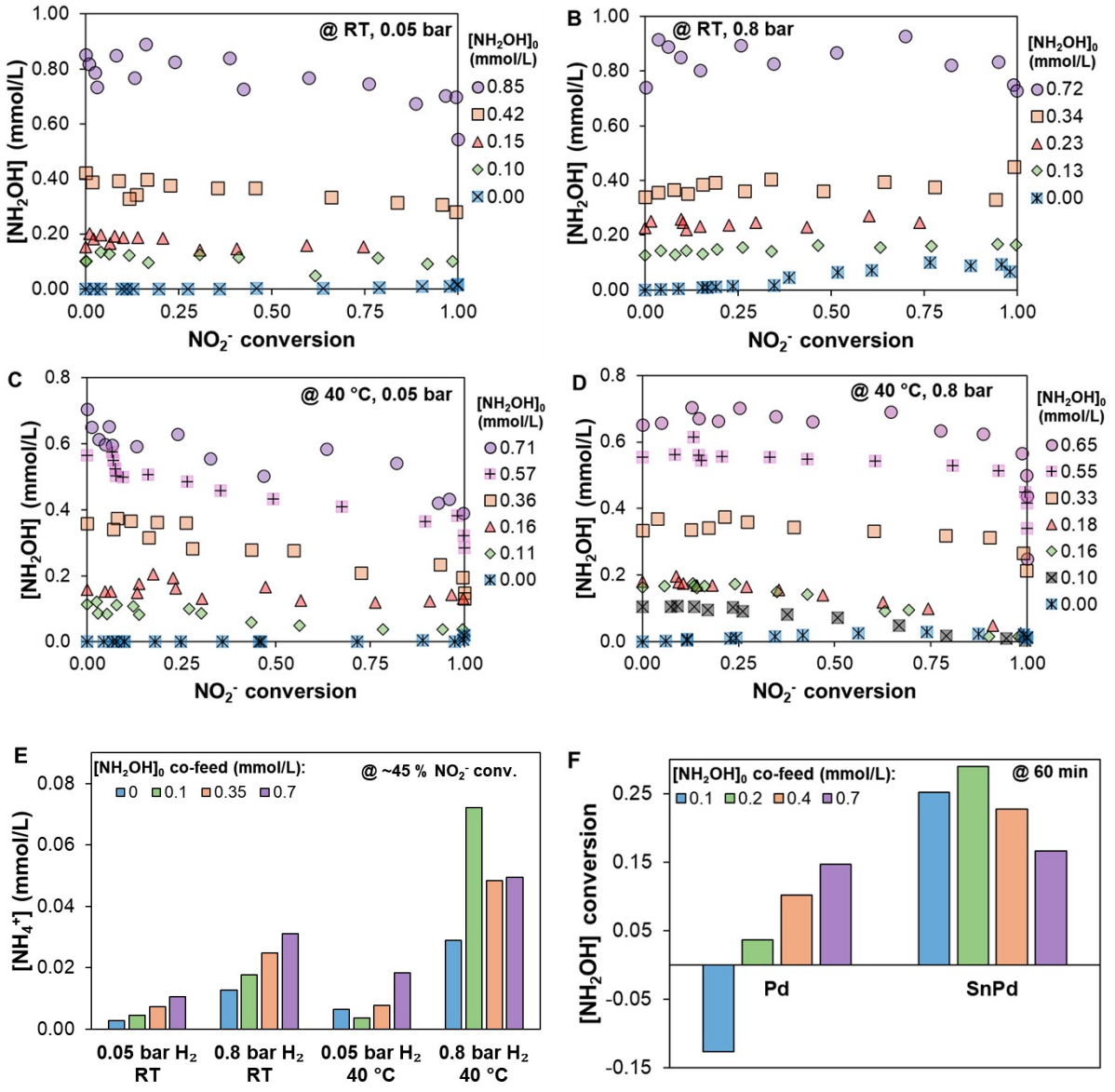

Figure 6: NH_2OH concentration as function of NO_2^- conversion at different NH_2OH co-feed concentrations at RT or 40 °C and at 0.8 or 0.05 bar H_2 (as stated in the chart, **A**-**D**), NH_4^+ concentration at different rounded NH_2OH co-feed concentrations at 45 % NO_2^- conversion (**E**) and comparison of NH_2OH conversion with Sn and SnPd catalyst at 0.8 bar after 60 min reaction (**F**). Negative NH_2OH conversion indicates net-NH_2OH formation. Reaction conditions: 300 mL H_2O, 0.8 mmol/L KNO_2, 10 mg Pd/Al_2O_3, 80 or 5 mL/ min H_2, 10 mL/min CO_2 and He to make up to 100 mL/min, RT or 40 °C, 600 rpm.

3. Unpublished AT-IR data by Rao et al. using isotope labeled NO_2^-

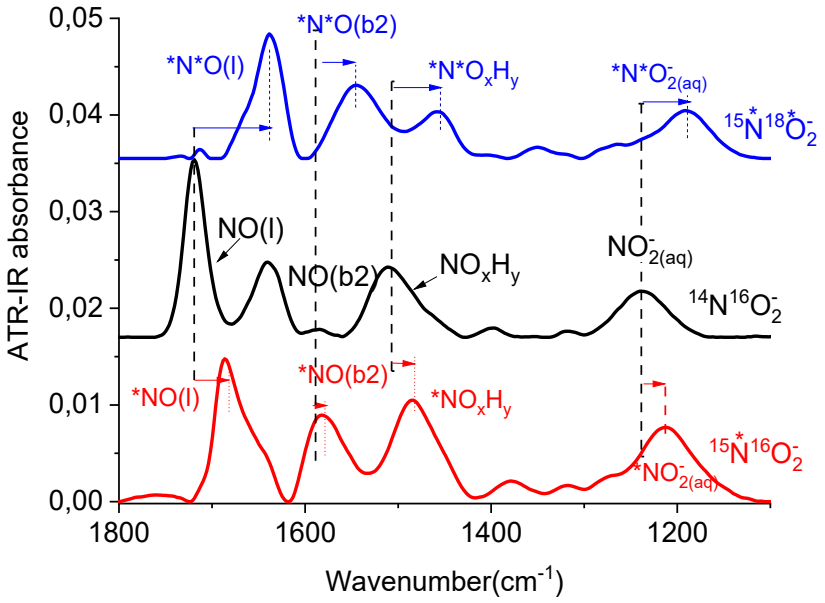

Figure 7: ATR-IR spectra of different nitrite isotopes ($^{14}N^{16}O_2^-$, $^{15}N^{16}O_2^-$, $^{15}N^{18}O_2^-$) during adsorption on H-Pd/Al_2O_3 at *t* = 30 min. Isotopic shifts are indicated by arrows.

The 1510 cm^{-1} band, also observed during decomposition of hydroxylamine on Pd/Al_2O_3 by Ebbesen *et al.*,[1,2] was previously assigned to the presence NH_2*. However, the peak at 1510 cm^{-1} observed with $^{14}N^{16}O_2^-$, shifts as a result of both isotope labels. Therefore, this species must contain both N and O, and therefore we propose NO_xH_y. Unfortunately, we can only conclude firmly the x cannot be zero. Whether the same is true for y, implying that the surface species contains H, is further discussed below.

The peak at 1510 cm^{-1}, could also be assigned to three-fold bonded NO, which would imply that y is zero. However, NO_xH_y is the preferred assignment because of two reasons. Firstly, the frequency is too low and the difference in wavenumbers between NO(b) and NO_xH_y is too large (70 cm^{-1}) to support the assignment to three-fold bonded NO. Secondly, adsorption of NH_2OH results in the formation of a very similar bond at 1510 cm^{-1}without any signal other adsorbed NO species,[1,2] clearly suggesting that hydrogen is present in NO_xH_y.

The remaining peak position obtained with labeled nitrite and shown in Figure 17 are summarized in Table 4. No peak shift was observed for the peak at 1640 cm^{-1}, confirming the assignment of this peak as originating from the H-O-H scissor band of water. For the peaks assigned to $NO_2^-{}_{(aq)}$, NO_xH_y, NO(b), NO(l) and NH_4^+ isotopic shifts are observed for both nitrogen- and oxygen-labeled nitrite, indicating that all these species contain both nitrogen and oxygen. For the peaks assigned to $NO_2^-{}_{(aq)}$ and NO(l) this is in line with previous assignments.

The peak assigned to NO(b) was not reported before and has a very low intensity. Actually, the intensity of this peak in the experiment with $^{14}N^{16}O_2^-$ is inaccurate as it can be easily

manipulated during the background subtraction, aiming at minimization of the 1640 cm^{-1} peak. The application of labeled nitrite clearly shows much more reliable observation of NO(b) thanks to the shift in the peak position.

Table 1: Summary of the observed peaks with different nitrite isotopes as shown in Figure 17.

Peak position/Assignment	$^{14}N^{16}O_2^-$ / cm^{-1}	$^{15}N^{16}O_2^-$ / cm^{-1}	$^{15}N^{18}O_2^-$ / cm^{-1}	peak ratio of $_{14}NO_2^-$ /$^{15}N^{16}O_2^-$	peak ratio of $^{14}NO_2^-$ /$^{15}N^{18}O_2^-$
$NO_2^-{}_{(aq)}$	1237	1211	1192	1.02	1.04
NO_xH_y	1510	1485	1458	1.02	1.04
NO(b2)	1584	1578	1558	1.00	1.02
NO(l)	1720	1686	1671	1.02	1.03
NH_4^+	1445	1418	1389	1.02	1.04
1640 cm^{-1}	1640	1640	1640	1	1

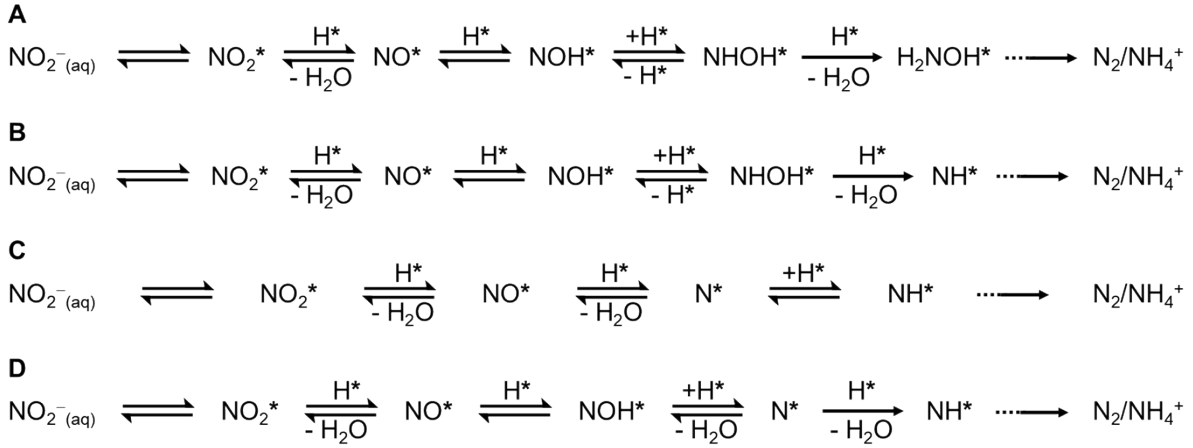

Figure 8: Four possible NO_2^- hydrogenation mechanisms on Pd/Al_2O_3 that fit the kinetic data based on microkinetic modelling by Xu.[3]

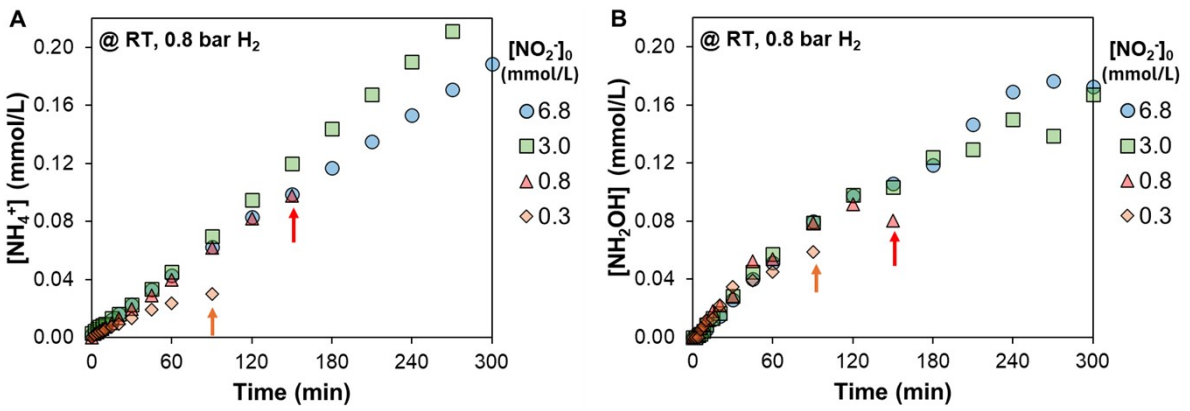

Figure 9: NH_4^+ concentration (**A**) and NH_2OH concentration (**B**) at RT as function of time at different initial NO_2^- concentrations. Arrows indicate time of full NO_2^- conversion, if reached. Reaction conditions: 300 mL H_2O, 10 mg $SnPd/Al_2O_3$, 80:10:10 mL/min H_2:CO_2:He, RT, 600 rpm.

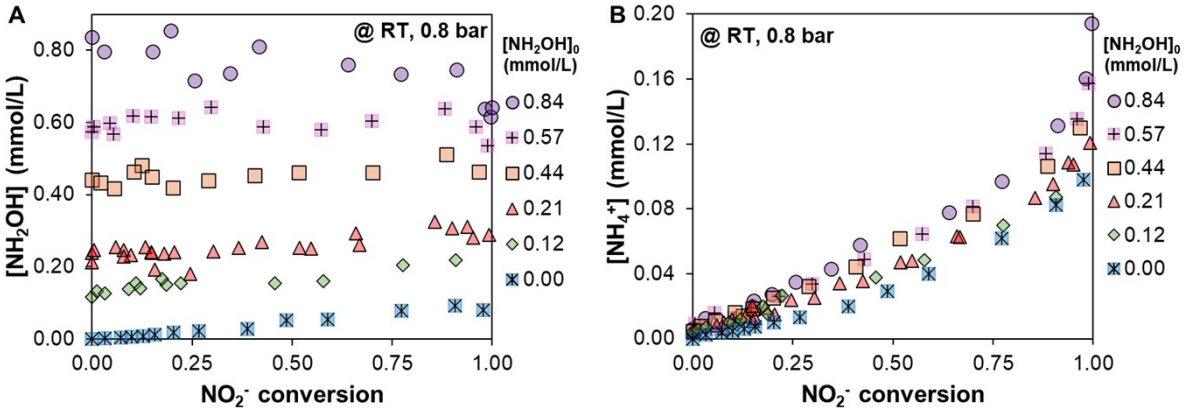

Figure 10: NH_2OH and NH_4^+ concentration as function of NO_2^- conversion at different NH_2OH co-feed concentrations at 0.8 bar H_2. Reaction conditions: 300 mL H_2O, 0.8 mmol/L KNO_2, 10 mg $SnPd/Al_2O_3$, 80:10:10 mL/min H_2:CO_2:He, RT, 600 rpm.

4. Langmuir–Hinshelwood Microkinetic Model Equations

In typical LH microkinetic modelling only one reaction line is considered. However, in this case HNOH* can originate either from NO_2^- or from NH_2OH. Therefore, the two extreme cases of (**1**) NH_2OH poor and (**2**) NH_2OH rich conditions are investigated. Under NH_2OH poor conditions the generation of HNOH from NH_2OH is neglected. For this case, Xu *et al.*[1] have already proven that the apparent reaction orders agree with experimental results for these conditions.

$H_2 + 2* \rightleftharpoons 2H*$ (equilibrium reaction 1, K_1)

$NO_2^- + * \rightleftharpoons NO_2*$ (equilibrium reaction 2, K_2)

$NO_2* + H* + H^+ \rightleftharpoons NO* + H_2O + *$ (equilibrium reaction 3, K_3)

NO* + H* ⇌ NOH* + * (equilibrium reaction 4, K_4)

NOH* + H* ⇌ HNOH* + * (equilibrium reaction 5, K_5) – dominant at NH_2OH poor conditions

NH_2OH* + * ⇌ NH_2OH* (equilibrium reaction 6, K_6)

NH_2OH* + * ⇌ HNOH* + H* (equilibrium reaction 7, K_7) – dominant at NH_2OH rich conditions

HNOH* + H* → NH* + H_2O + * (reaction 8, k_8, RDS)

We assume reaction 8 as the RDS. So, the Pd surface species are H*, NO_2^-*, NO*, NOH*, HNOH*, NH_2OH*:

$$\theta_H = K_1^{0.5}[H_2]^{0.5}\theta^*$$

$$\theta_{NO_2^-} = K_2[NO_2^-]\theta^*$$

$$\theta_{NO} = K_1^{0.5}K_2K_3[H^+][NO_2^-][H_2]^{0.5}\theta^*$$

$$\theta_{NOH} = K_1K_2K_3K_4[H^+][NO_2^-][H_2]\theta^*$$

$$\theta_{HNOH\_1} = K_1^{1.5}K_2K_3K_4K_5[H^+][NO_2^-][H_2]^{1.5}\theta^*$$ relevant for NH_2OH poor conditions

$$\theta_{NH_2OH} = K_6[NH_2OH]\theta^*$$

$$\theta_{HNOH\_2} = \frac{K_6K_7[NH_2OH]\theta^*}{K_1^{0.5}[H_2]^{0.5}}$$ relevant for NH_2OH rich conditions

$$\theta_{HNOH} = K_1^{1.5}K_2K_3K_4K_5[H^+][NO_2^-][H_2]^{1.5}\theta^* + \frac{K_6K_7[NH_2OH]\theta^*}{K_1^{0.5}[H_2]^{0.5}}$$

Scenario 1: Under NH_2OH poor conditions the contribution of the red term is much bigger than the one of the green one, so we can neglect the green term and use θ_{HNOH_1} for θ_{HNOH}:

Site balance:

$$1 = \theta_H + \theta_{NO_2^-} + \theta_{NO} + \theta_{NOH} + \theta_{HNOH\_1} + \theta^*$$

$$\theta^* = \frac{1}{1 + K_1^{0.5}[H_2]^{0.5} + K_2[NO_2^-] + K_1^{0.5}K_2K_3[H^+][NO^{2-}][H_2]^{0.5} + K_1K_2K_3K_4[H^+][NO_2^-][H_2] + K^{1}}$$

$$Rate = k_8\theta_H\theta_{HNOH} = k_8K_1^{0.5}[H_2]^{0.5}\theta^* K_1^{1.5}K_2K_3K_4K_5[H^+][NO_2^-][H_2]^{1.5}\theta^* = K_1K_2K_3K_4K_5k_8[H^+][NO_2^-][$$

At low H_2 pressure, we cross out the products containing $[H_2]$ in the denominator and rewrite:

$$Rate = \frac{K_1^{1.5} K_2 K_3 K_4 K_5 k_8 [H^+][NO_2^-][H_2]^2}{\left(1 + K_2[NO_2^-]\right)^2}$$

Thus, at low H_2 pressure the order in H_2 is 2 and the order in NO_2^- is [-1, 1].

At high H_2 pressure we can ignore $K_2[NO_2^-]$ and can rewrite:

$$Rate == \frac{K_1^2 K_2 K_3 K_4 K_5 k_8 [H^+][NO_2^-][H_2]^2}{\left(1 + K_1^{0.5}[H_2]^{0.5} + K_1^{0.5} K_2 K_3 [H^+][NO^{2-}][H_2]^{0.5} + K_1 K_2 K_3 K_4 [H^+][NO_2^-][H_2] + K^{\cdots}\right.}$$

Thus, at high H_2 pressure the order in H_2 can vary from [-1, 2] and the order in NO_2^- can vary from [-1, 1]. This covers the entire range observed in this work and in earlier works of Huang *et al*. and Xu *et al*..[3]

Scenario 2: Under NH_2OH rich conditions the contribution of the green term is much bigger than the one of the red one, so we can neglect the red term and use θ_{HNOH_2} for θ_{HNOH}:

Site balance:

$$1 = \theta_H + \theta_{NO_2^-} + \theta_{NO} + \theta_{NOH} + \theta_{HNOH\_2} + \theta^*$$

$$\theta^* = \frac{1}{1 + K_1^{0.5}[H_2]^{0.5} + K_2[NO_2^-] + K_1^{0.5} K_2 K_3 [H^+][NO^{2-}][H_2]^{0.5} + K_1 K_2 K_3 K_4 [H}$$

$$Rate = k_8 \theta_H \theta_{HNOH} = k_8 K_1^{0.5}[H_2]^{0.5} \theta^* \frac{K_6 K_7 [NH_2OH]\theta^*}{K_1^{0.5}[H_2]^{0.5}} = K_6 K_7 k_8 [NH_2OH]\theta^{*2} = \frac{}{\left(1 \right.}$$

At low H_2 pressure, we cross out the products containing $[H_2]$ in the denominator and rewrite:

$$Rate = \frac{K_6 K_7 k_8 [NH_2OH]}{\left(1 + K_2[NO_2^-] + \frac{K_6 K_7 [NH_2OH]}{K_1^{0.5}[H_2]^{0.5}}\right)^2}$$

Crossing out $[H_2]$ as only term in the denominator is mathematically forbidden so we remain with a fractional term in the denominator and cannot straight forwardly define reaction orders for H_2. However, the rate law suggests that the rate decreases with decreasing H_2 pressure which meets the observation. The reaction order for NO_2^- is [-1, 0] and the order in NH_2OH [-1, 1] which covers the experimental observation (0^{th} order in NO_2^- and NH_2OH).

At high H_2 pressure we can ignore $K_2[NO_2^-]$ and can rewrite:

$$Rate == \frac{K_6 K_7 k_8 [NH_2OH]}{\left(1 + K_1^{0.5}[H_2]^{0.5} + K_1^{0.5} K_2 K_3 [H^+][NO^{2-}][H_2]^{0.5} + K_1 K_2 K_3 K_4 [H^+][NO_2^-]\right.}$$

Thus, at high H_2 pressure we remain with the same problem and cannot straight forwardly define reaction orders for H_2 from this expression. The orders for NO_2^- and NH_2OH remain at [-1, 0] and [-1, 1], respectively.

5. References

1 S. D. Ebbesen, B. L. Mojet and L. Lefferts, *Langmuir*, 2008, **24**, 869–879.

2 S. D. Ebbesen, B. L. Mojet and L. Lefferts, *J Catal*, 2008, **256**, 15–23.

3 P. Xu, S. Agarwal and L. Lefferts, *J Catal*, 2020, **383**, 124–134.